Optimal Control of Heat Transfer and Skin Friction in Wall Turbulence

M. Yokoo[1], N. Kasagi[1], and Y. Suzuki[1]

[1]*Department of Mechanical Engineering, The University of Tokyo, Hongo, Bunkyo-ku, Tokyo 113-8656, Japan*

Abstract - Optimal control theory based on the Frechet derivative of a cost function was applied to simultaneous control of turbulent heat transfer and skin friction with local blowing/suction on the wall, and its performance was evaluated by using a direct numerical simulation of a turbulent channel flow. Spatio-temporal relationship between the near-wall coherent structures and the distribution of control input is examined in detail for different cost function. It is found that the control input optimized for drag reduction and that for heat transfer augmentation are mostly 180 degrees out-of-phase each other, when the wall-normal gradients of velocity and temperature are directly employed in the cost function. On the other hand, the distribution of control input aiming at reducing turbulent intensity is very similar to that for the v-control scheme (Choi et al., 1994), and is mostly 180 degrees out of phase with the control input aiming at increasing temperature variance. By employing the wall-normal gradients of velocity and temperature simultaneously in the cost function, heat transfer augmentation is achieved with a smaller expense of the skin friction.

1. Introduction

Management of turbulent flow and associated scalar transport in various engineering applications should lead to significant benefits for saving energy and protecting the environment. Due to the inherent similarity between momentum and scalar transport especially in the vicinity of the wall[1, 2], it is difficult to achieve drag reduction and heat transfer augmentation simultaneously, when conventional control methodologies are employed.

Recently, active feedback control attracts much attention because of its marked control effect with small energy input[3, 4]. Among various control schemes, the optimal control theory based on the Frechet derivative[5] of a cost function is one of the most powerful techniques. Bewley et al.[6] applied a suboptimal control procedure to turbulent channel flow and obtained about 17% drag reduction in their direct numerical simulation (DNS). Lee et al.[7] derived an analytical solution of the suboptimal control through the Fourier transform. The computational load for determining the control input is significantly reduced, and 22% drag reduction is obtained. Moin & Bewley[8] applied an optimal control procedure to turbulent channel flow and found over 50% drag reduction.

The objectives of the present study are to apply the optimal control theory to simultaneous control of velocity and thermal fields, and to evaluate its performance through DNS of a fully-developed turbulent channel flow. Spatio-temporal relationship between the control input and the near-wall coherent structures is also investigated in detail.

2. Problem Formulation and Numerical Procedure

The problem under consideration is a turbulent channel flow with heat transfer, where the two walls are kept isothermal, but at different temperatures. The governing equations are the incompressible Navier-Stokes equation, the continuity equation, and the energy equation, i.e.,

$$\frac{\partial u_i}{\partial t} + u_j \frac{\partial u_i}{\partial x_j} = -\frac{\partial p}{\partial x_i} + \frac{1}{Re_\tau} \frac{\partial^2 u_i}{\partial x_j \partial x_j}, \qquad \frac{\partial u_i}{\partial x_i} = 0, \tag{1}$$

$$\frac{\partial \theta}{\partial t} + u_j \frac{\partial \theta}{\partial x_j} = \frac{1}{Pe} \frac{\partial^2 \theta}{\partial x_j \partial x_j}, \qquad Pe = Re_\tau \cdot Pr, \tag{2}$$

where x_1, x_2, and x_3 are the streamwise, wall-normal, and spanwise directions, respectively. The quantities are non-dimensionalized with the wall friction velocity u_τ, the channel half-width δ, and the temperature difference between two walls. Periodic boundary condition is employed in the x_1- and x_3- directions for the velocity and thermal field. As a control input ϕ, local blowing/suction is assumed on the wall, and is written as:

$$u_2\big|_{wall} = \phi(x_1, x_3, t). \tag{3}$$

The Reynolds Number Re_τ based on u_τ and δ is 100, while the Prandtl number Pr is 0.71.

A second-order finite difference scheme and a fractional step method[9] are employed for the spatial and temporal discretization, respectively. The number of grids is chosen as $96\times129\times96$ with a computational domain of $2.5\pi\delta\times2\delta\times\pi\delta$ in the x_1-, x_2-, and x_3- directions. Fully-developed turbulent flow is chosen as the initial condition and the flow rate is kept constant during the present calculation.

3. Optimal Control Procedure

The control input ϕ is determined by the same procedure as Moin & Bewley[8], so as to minimize the cost function. With their procedure, the Navier-Stokes equation is integrated from $\tau=0$ to $\tau=T$, and then the adjoint equation is solved backward from $\tau=T$ to $\tau=0$ in order to calculate ϕ. The optimum distribution ϕ is determined by repeating this cycle until it converges. The cost function to be minimized in the present study is defined as follows:

$$J(\phi)=\frac{1}{2}\int_w\int_0^T\phi^2 d\tau dS+\frac{l}{2}\int_w\int_0^T\left(\frac{\partial u_1}{\partial x_2}\right)^2 d\tau dS-\frac{m}{2}\int_w\int_0^T\left(\frac{\partial\theta}{\partial x_2}\right)^2 d\tau dS$$

$$+\frac{h}{2}\int_V u_i' u_i'\big|_{\tau=T} dV-\frac{k}{2}\int_V \theta'^2\big|_{\tau=T} dV\,, \tag{4}$$

where l, m, h and k are the weighting factors, while u_i' and θ' denote the fluctuating velocity and temperature, respectively. The first term represents the cost for control. The second and third terms are respectively the measures of wall friction and heat transfer integrated over the wall surface and a finite time period *T*. On the other hand, the fourth and fifth terms are the measures evaluated at the end of the control period, and correspond to the volume integral of the turbulent kinetic energy and that of the temperature variance, respectively. The time period of the optimal control should be large enough if compared with the characteristic time scale of the near-wall coherent structures to be controlled. However, since it is necessary to store all the instantaneous flow field to solve the adjoint equation, *T* is chosen as 16 viscous time units in the present study due to the limitation of the computer memory.

In the following section, we first set each of the weighting factors in Eq. (1) to be nonzero, and evaluate the optimal control of skin friction and that of heat transfer independently. Then, the simultaneous control of heat transfer and skin friction is examined by employing non-zero values for two weighting factors at the same time.

4. Computational Result

The weighting factors adopted in the present study and the resultant statistics are summarized in Table 1. The weighting factors listed in Table 1 are determined in such a way that the cost for control (the first term in Eq. 4) at the initial time instant is same as that for the active cancelation (v-control, hereafter)[10]. In the present study, the control input in v-control is determined as $\phi=-u_2\big|_{y^+=10}$. Figure 1 shows time traces of the skin friction coefficient C_f, and the Nusselt number Nu, in Cases A and C, which are normalized with those in the case of the

Table 1: Weighting factors and resultant statistics for controlled cases examined.

Case	l	m	k	h	$\phi_{rms}\|_{t=0}$	$(C_f - C_{f0})/C_{f0}$	$(Nu - Nu_0)/Nu_0$
A	7.5×10^{-5}	0.0	0.0	0.0	1.75×10^{-1}	-11.7	-11.5
B	0.0	2.8×10^{-1}	0.0	0.0	1.79×10^{-1}	33.0	26.7
C	0.0	0.0	6.0×10^{-4}	0.0	9.01×10^{-2}	-19.5	-20.7
D	0.0	0.0	0.0	9.8×10^{-1}	9.01×10^{-2}	13.1	11.7
E	3.0×10^{-4}	1.0	0.0	0.0	1.83×10^{-1}	-2.27×10^{-3}	6.34×10^{-3}
F	1.0×10^{-4}	0.0	0.0	1.5	1.82×10^{-1}	4.12×10^{-2}	5.36×10^{-2}

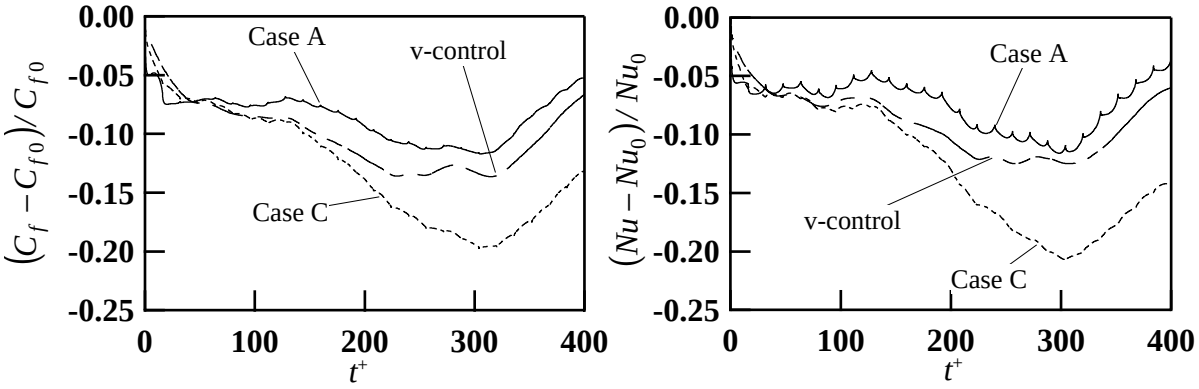

Figure 1: Time traces of the relative changes in Nu and C_f.

unmanipulated flow. For comparison, C_f and Nu obtained in v-control are also plotted. By repeating the optimal control time period of $T^+ = 16$, C_f and Nu are decreased by about 10% in Case A and about 20% in Case C, respectively. On the other hand, C_f and Nu are increased by almost the same amount for both Cases B and D as listed in Table 1. In Cases A and C, the cost for control is smaller than that of v-control by about 70% and about 50%, respectively. Thus, the present optimal control should give substantial control effects with relatively small control input, although the optimal time period are much shorter than that employed by Moin & Bewley[8]($T^+ = 100$).

Figure 2 shows an instantaneous velocity field in the *y*-*z* plane, and the control input normalized by its rms value. For comparison, the distributions of the control input derived from the v-control and the suboptimal control procedure[7] are also plotted in Fig. 2(b). The cost function of the suboptimal control is chosen as,

$$J = \frac{1}{2}\int_w \phi^2 dS + \frac{l}{2}\int_w \left(\frac{\partial u_1}{\partial x_2}\right)^2 dS\,, \tag{5}$$

which is the same as the present one, whilst the time integral in Eq. (4) is omitted.

In Fig. 2(a), a near-wall streamwise vortex is observed at around $x_3^+ = 130$. The blowing/suction rate on the wall determined with the v-control is 180 degrees out-of-phase with the wall-normal velocity at $x_2^+ = 10$ as designed. The present control for Case A gives a similar distribution with that of the v-control, so that effective control is expected through selective manipulation of the streamwise vortices. However, the control input determined with the suboptimal control procedure of Lee et al.[7] exhibits a different trend; ϕ is in phase with u_2' in the buffer layer. Therefore, as Lee et al.[7] reported, their procedure is inappropriate when the skin friction is directly included in the cost function.

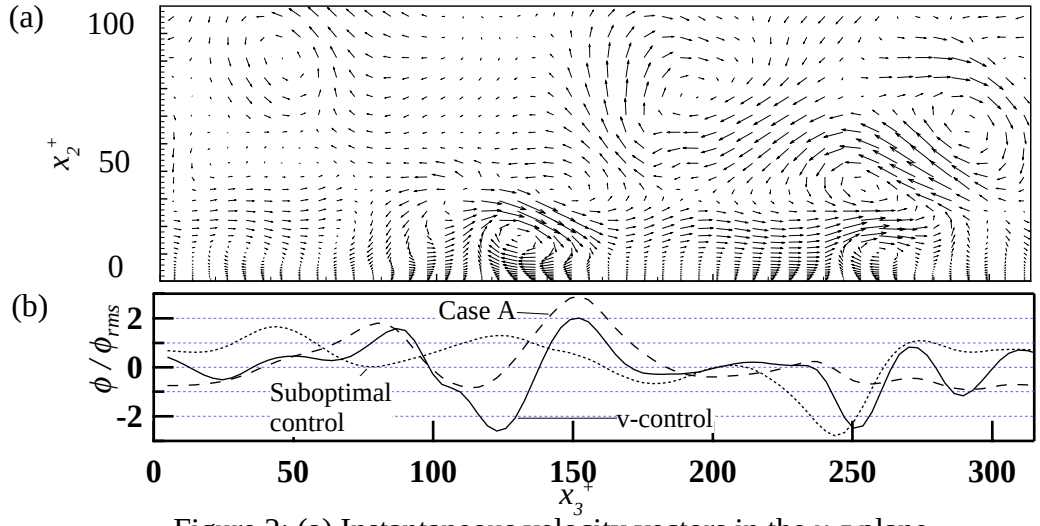

Figure 2: (a) Instantaneous velocity vectors in the *y*-*z* plane.
(b) Spanwise distribution of control input.

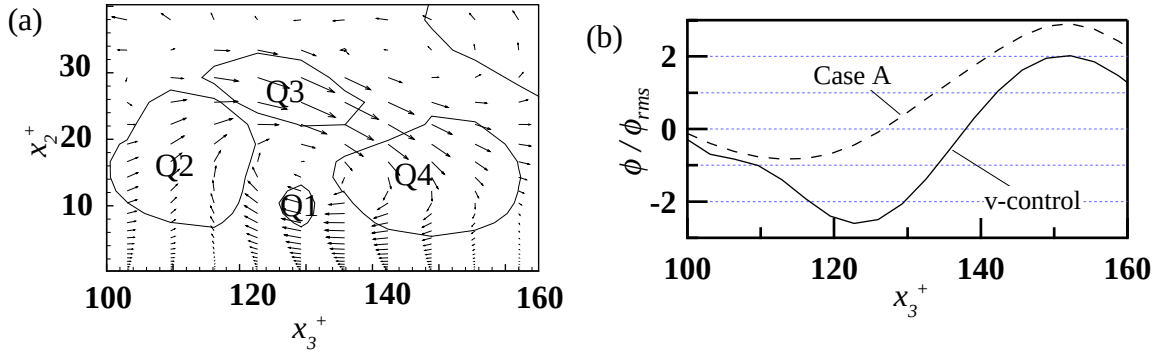

Figure 3: (a) Magnified view of the instantaneous velocity vectors of Fig. 2(a) and contour lines of $\left|u'v'/u_\tau^2\right|$=0.5. (b) Distributions of control input.

Figure 3(a) shows a magnified view of the velocity vectors around the streamwise vortex and the regions of large shear products $u_1'u_2'$. As reported by previous studies[11, 12], the sweep (Q4) and ejection (Q2) events occur on the downwash and upwash sides of the vortex, respectively. On the other hand, a region of strong outward interaction (Q1) exists underneath the vortex. Although the control input in Case A is in accordance with that of the v-control in the regions of the Q2 and Q4 events, it exhibits a different trend near the Q1 event as shown in Fig. 3(b). It is also noted that the magnitude of blowing in Case A is generally larger than that for the v-control, whilst suction is smaller in both control cases. Moreover, the area where suction is applied in Case A occupies about 60% of the wall surfaces as described later in Fig. 4(a), which is larger than that for the v-control.

Figure 4 shows the temporal evolution of the control input ϕ in Case A. The regions of strong blowing/suction are elongated in the streamwise direction, and aligned side by side in the spanwise direction. Although the magnitude of blowing/suction rate is decreased with time, the spatial distribution of ϕ is unchanged qualitatively. It is also found that these regions propagate at a speed of $U_c^+ \approx 10$, which is in accordance with the propagation velocity for u_1' near the wall[13]. Therefore, the present optimal control in Case A should selectively apply the control input to the near-wall coherent structures.

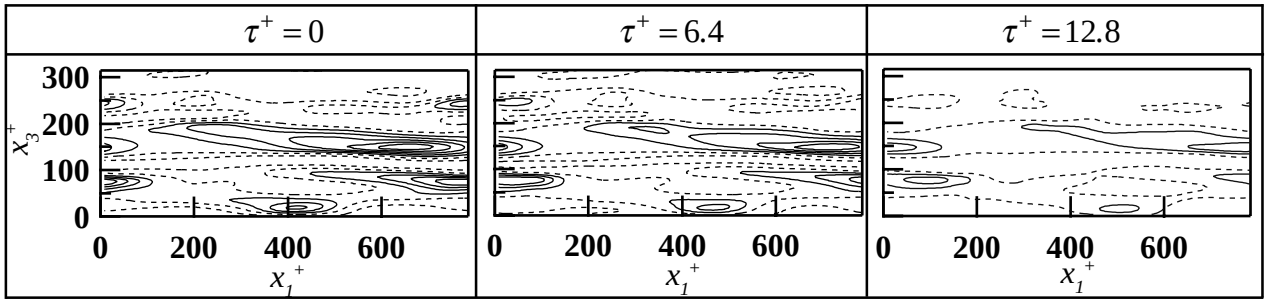

Figure 4: Temporal evolution of the control input in Case A. Negative contours are dashed. The contour levels range from ϕ / u_τ = -0.6 to 0.6.

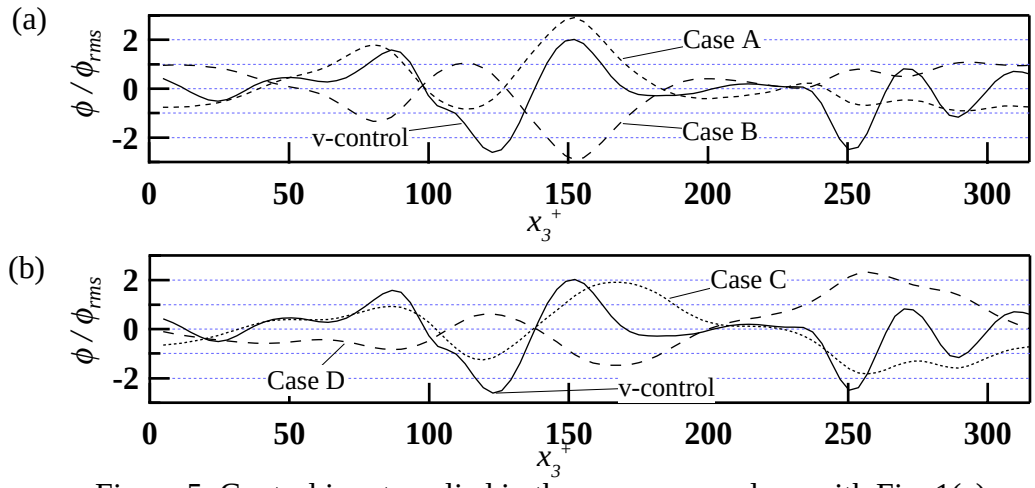

Figure 5: Control input applied in the same $y-z$ plane with Fig. 1(a).

The control target for Case B is to enhance the heat transfer on the wall ($m \neq 0$, $l = h = k = 0$). Figure 5(a) shows the control input determined for the same cross-section as in Fig. 2(a). It is striking that the control input for Cases A and B is mostly 180 degrees out-of-phase. This is because, due to the inherent similarity between heat and momentum transfer near the wall, the regions of large turbulent heat flux ($-u_2'\theta'$) correspond well to those of large Reynolds shear stress. As in Case A, the regions of strong blowing/suction are elongated in the streamwise direction, and have a propagation velocity of about $U_c^+ \approx 10$, although the sign of ϕ is opposite in most regions.

In Case C, the turbulent kinetic energy at the end of control period is included in the cost function ($h \neq 0$, $l = m = k = 0$). Figure 5(b) shows the control input determined for the same cross-section as Fig. 2(a). It can be said that the distribution of control input for Case C is very similar to that of v-control in the region close to the isolated streamwise vortex. However, in the region where several vortices interact with each other (at around $x_3^+ = 270$), the control input of Case C is different from that of v-control. In Case D, the temperature variance is included in the cost function ($k \neq 0$, $l = m = h = 0$). It can be observed in Fig. 5(b) that the control input for Cases C and D are again mostly 180 degrees out-of-phase. Although it is not shown here, the regions of strong blowing/suction are elongated in the streamwise direction as in Cases A and B, and have the same propagation velocity of about $U_c^+ \approx 10$.

It is now clear that separate control of skin friction and heat transfer presently examined preserves similarity between heat and momentum transfer. In the following section, possibility of the dissimilarity is examined by employing two terms of RHS of Eq. (4) simultaneously.

Table 2: Octant analysis[14]

1st octant	$u'>0,v'>0,\theta'<0$	cold outward interaction	5th octant	$u'>0,v'>0,\theta'>0$	hot outward interaction
2nd octant	$u'<0,v'>0,\theta'<0$	cold ejection	6th octant	$u'<0,v'>0,\theta'>0$	hot ejection
3rd octant	$u'<0,v'<0,\theta'<0$	cold wallward interaction	7th octant	$u'<0,v'<0,\theta'>0$	hot wallward interaction
4th octant	$u'>0,v'<0,\theta'<0$	cold sweep	8th octant	$u'>0,v'<0,\theta'>0$	hot sweep

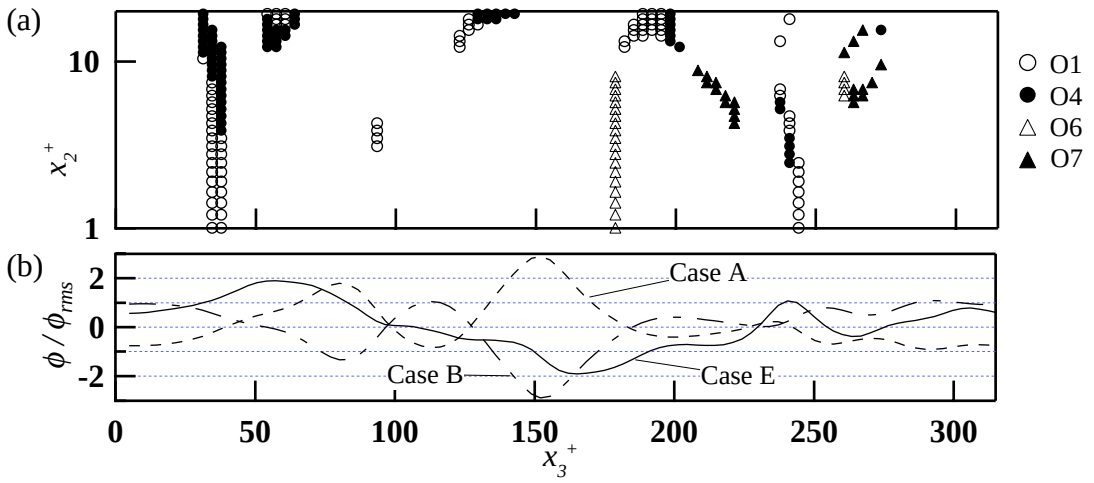

Figure 6: (a) Distribution of O1, O4, O6 and O7 in the same $y-z$ plane with Fig. 2(a). (b) Spanwise distributions of control input.

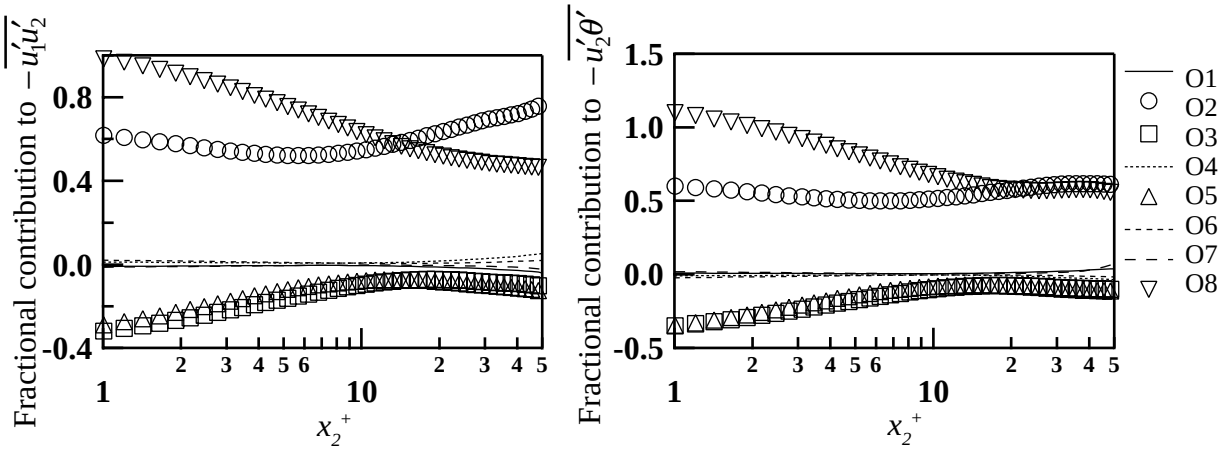

Figure 7: Fractional Contribution to $-\overline{u_1'u_2'}$ and $-\overline{u_2'\theta'}$ from each octant.

Suzuki et al.[14] propose conditional analysis ("octant analysis") by taking into account the signs of u_1', u_2' and θ', in order to investigate the detailed mechanism of the turbulent heat transfer. Instantaneous velocity and temperature fluctuations are classified into eight events (O1-O8) as shown in Table 2. Events in the 2nd, 4th, 6th and 8th octant contribute positively to $-u_1'u_2'$, whilst those in the 1st, 3rd, 5th or 7th octant negatively to $-u_1'u_2'$. On the other hand, events in the 1st, 2nd, 7th or 8th octants contribute positively to $-u_2'\theta'$, whilst those in the 3rd, 4th, 5th or 6th octant negatively to $-u_2'\theta'$. Thus, cold ejection (O2) and hot sweep (O8) always make positive contribution to both heat and momentum transfer. Cold wallward interaction (O3) and hot outward interaction (O5) have negative contribution to both heat and momentum transfer. All of these events contribute to similarity between velocity and thermal field. On the other hand, the other four events (O1, O4, O6, O7) contribute to the heat and momentum transfer

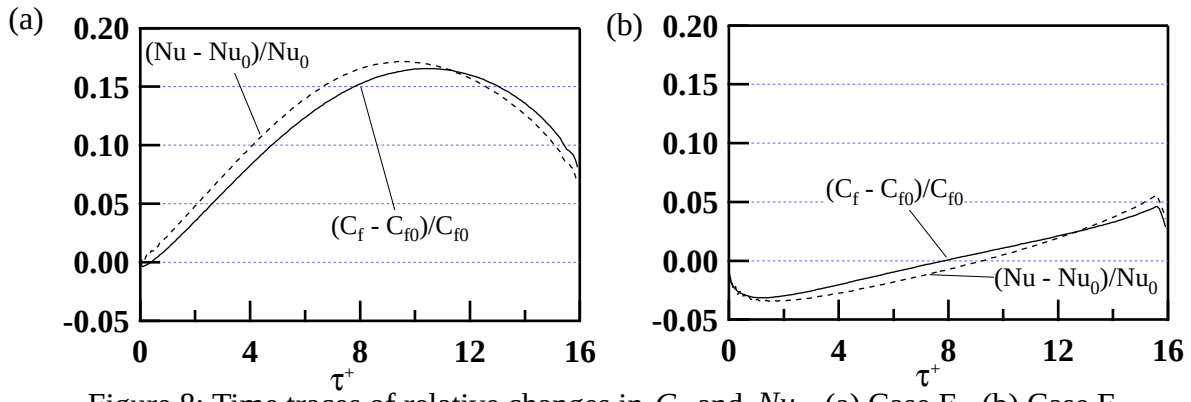

Figure 8: Time traces of relative changes in C_f and Nu. (a) Case E, (b) Case F.

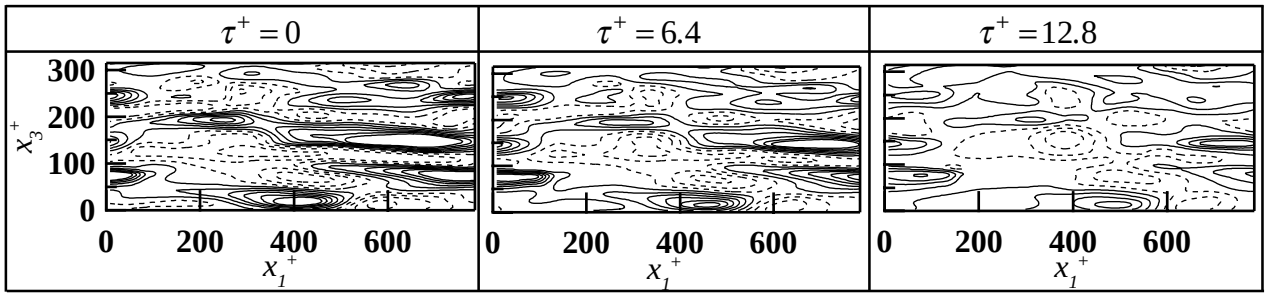

Figure 9: Temporal evolution of the control input in Case F. Negative contours are dashed. The contour levels range from ϕ / u_τ = -0.4 to 0.4.

in the opposite way. Therefore, dissimilarity between turbulent transport of heat and momentum can be expected when these events are strengthened through the present control.

Figure 6(a) shows the distribution of O1, O4, O6 and O7 in the same $y-z$ plane as in Fig. 2(a). Although we could expect substantial dissimilarity between heat and momentum transfer when these events are active, it is shown in this figure that they are rather sparsely distributed in space. Moreover, as shown in Fig. 7, their fractional contribution to the Reynolds stress and the turbulent heat flux is negligibly small if compared with the other events having positive contribution to the similarity.

Figure 6(b) shows the distribution of ϕ in Cases A, B, and E, where ϕ is normalized by its rms value in each case. The control input in Case E has peaks at the spanwise location where that of Cases A and B is in phase. These regions correspond well to O1, O4, O6 and O7. It is also indicated that the control input in these regions has the same sign of u_2' near the wall, which might strengthen these events.

Figure 8 shows time traces of C_f and Nu in Cases E and F. In Case E, both C_f and Nu are increased, so that substantial dissimilarity between heat and momentum transfer is not derived in this case, either. However, at $\tau^+ < 10$, Nu is increased by a somewhat larger amount than that for C_f. In Case F, the relative changes for both Nu and C_f are gradually increased, but the changes in C_f is smaller than that for Nu.

Figure 9 shows the temporal evolution of the control input in Case F. At $\tau^+ = 0$, the distribution of the control input is similar to that of Case A. However, at $\tau^+ > 6.4$, the regions having large blowing/suction rate exist near the strong vortices, and can be divided into two different groups. One group exhibits similar distribution with that in Case A, where ϕ is opposite to u_2' induced by the vortices. On the other hand, ϕ in the another group is in phase with the u_2'. Therefore, the distribution of the control input for Case F consists of patches of those for Cases A and D.

5. Conclusion

The optimal control theory based on the Frechet derivative of the cost function was applied to simultaneous control of heat transfer and skin friction by using local blowing/suction on the wall. Various kinds of cost function were examined and their performance was evaluated by using direct numerical simulation of a turbulent channel flow. The following conclusions can be derived:

1) The control input optimized for drag reduction is similar to that determined by v-control, and is 180 degrees out-of-phase with the wall-normal velocity in the buffer layer. On the other hand, the control input optimized for heat transfer augmentation is mostly in-phase with it.
2) The distribution of the control input aiming at reducing turbulent intensity is similar to that of v-control, and this input is mostly 180 degrees out-of-phase with the control input aiming at increasing temperature variance.
3) The inherent similarity between velocity and thermal field in the near-wall region is preserved when separate control for the heat transfer or the skin friction is applied. However, when the measures of heat transfer and skin friction are simultaneously employed in the cost function, heat transfer augmentation can be obtained with a smaller expense of the skin friction, although the magnitude of the dissimilarity is somewhat small in the control cases presently examined.

Reference

[1] N. Kasagi, Y. Tomita, and A. Kuroda. Direct numerical simulation of the passive scalar field in a turbulent channel flow. Trans. ASME: *J. Heat Transfer*., **114**, pp. 598-606, 1992.

[2] N. Kasagi and Y. Ohtsubo. Direct Numerical Simulation of Low Prandtl Number Thermal Field in a Turbulent Flow. *Turbulent Shear Flows*, **8**, Springer-Verlag, pp. 97-119, 1993.

[3] P. Moin and T. Bewley. Feed back control of turbulence. *Appl. Mech. Rev*. **47**-6, pp. S3-S13, 1994.

[4] N. Kasagi and O. Iida. Progress in Direct Numerical Simulation of Turbulent Heat Transfer. *Keynote Paper, 5th ASME/JSME Joint Thermal Engineering Conference, San Diego, CD-ROM Publication, ASME, March*, 1999.

[5] B. A. Finlayson. *The Method of Weighted Residuals and Variational Principles.* Academic Press, New York, 1972.

[6] T. Bewley, H. Choi, R. Temam and P. Moin. Optimal feedback control of turbulent channel flow. *CTR Annual Research Briefs*, pp. 3-14. 1993.

[7] C. Lee, J. Kim, and H. Choi. Suboptimal control of turbulent channel flow for drag reduction. *J. Fluid Mech.*, **358**, pp. 245-258, 1998.

[8] P. Moin and T. Bewley. Application of control theory to turbulence. *Proc 12th Australian Fluid Mech. Conf., Sydney, Australia*, PP. 10-15, 1995.

[9] M. M. Rai and P. Moin. Direct simulations of turbulent flow using finite-different schemes. *J. Comput. Phys*., **96**, pp. 15-53, 1991.

[10] H. Choi, P. Moin and J. Kim. Active turbulence control for drag reduction in wall-bounded flows. *J. Fluid Mech.*, **262**, pp. 75-110, 1994.

[11] S. K. Robinson. The kinematics of turbulent boundary layer structure. *Annu. Rev. Fluid Mech*., **23**, pp. 601-639, 1991.

[12] N. Kasagi, Y. Sumitani, Y. Suzuki, and O. Iida. Kinematics of the Quasi-Coherent Vortical Structure in Near-Wall Turbulence. *Int. J. Heat & Fluid Flow*, **16**(1), pp. 2-10, 1995.

[13] J. Kim and F. Hussain. Propagation velocity of perturbations in turbulent channel flow. *Phys. Fluids*. **A 5(3)**, pp. 695-706, 1993.

[14] H. Suzuki, K. Suzuki and T. Sato. Dissimilarity between heat and momentum transfer in a turbulent boundary layer disturbed by a cylinder. *Int. J. Heat Mass Transfer*., **31**-2, pp. 259-265, 1988.